

# Hierarchical Bayesian Nearest Neighbor Co-Kriging Gaussian Process Models; An Application to Intersatellite Calibration

Si Cheng<sup>1</sup>, Bledar A. Konomi<sup>1</sup>, Jessica L. Matthews<sup>2</sup>, Georgios Karagiannis<sup>3</sup>,  
and Emily L. Kang<sup>1</sup>

<sup>1</sup>University of Cincinnati

<sup>2</sup>North Carolina State University, Cooperative Institute for Satellite Earth System Studies (CISESS)

<sup>3</sup>Durham University

October 26, 2021

## Abstract

Recent advancements in remote sensing technology and the increasing size of satellite constellations allows massive geophysical information to be gathered daily on a global scale by numerous platforms of different fidelity. The auto-regressive co-kriging model is a suitable framework to analyse such data sets because it accounts for cross-dependencies among different fidelity satellite outputs. However, its implementation in multifidelity large spatial data-sets is practically infeasible because the computational complexity increases cubically with the total number of observations. In this paper, we propose a nearest neighbor co-kriging Gaussian process that couples the auto-regressive model and nearest neighbor GP by using augmentation ideas. Our model reduces the computational complexity to be linear with the total number of spatial observed locations. The latent process of the nearest neighbor GP is augmented in a manner which allows the specification of semi-conjugate priors. This facilitates the design of an efficient MCMC sampler involving mostly direct sampling updates which can be implemented in parallel computational environments. The good predictive performance of the proposed method is demonstrated in a simulation study. We use the proposed method to analyze High-resolution Infrared Radiation Sounder data gathered from two NOAA polar orbiting satellites.

Keywords: Augmented hierarchically nested design, Autoregressive Co-kriging, Nearest neighbor Gaussian process, Remote sensing

# 1 Introduction

Nowadays, due to the advancement of remote sensing technology, and the increasing size of satellite constellations, it has become common that geophysical information is measured by numerous platforms at the same time and place. Due to aging and exposure to the harsh environment of space, sensor degradation occurs over the satellite lifetime causing a decrease on performance reliability. This results in inaccuracy of the data as a true measure for long term trend analysis (Goldberg, 2011). For instance, newer satellites with more advanced sensors usually provide information of higher fidelity than the older ones, even if one employs standard intersatellite calibration such as those in (Cao et al., 2004, 2005). Consequently, different platforms often have large amounts of observations with varying fidelity for spatial areas that may or may not overlap or have the same spatial footprint. A single composite feature which includes adequate information from multiple data sources is preferred for statistical inference.

Co-kriging is a well established concept in geostatistics which can be used to analyse spatially correlated random processes (Davis and Greenes, 1983; Aboufirassi and Mariño, 1984; Ver Hoef and Cressie, 1993; Furrer and Genton, 2011; Genton and Kleiber, 2015). Complex cross-covariance functions can lead to infeasible computational complexity, even in the presence of moderate amount of data. To address this issue Kennedy and O'Hagan (2000) proposed an autoregressive co-kriging model which is simple, but yet flexible, to model complex dependency structure. The autoregressive co-kriging framework has gained popularity in computer experiments (Qian and Wu, 2008; Han et al., 2010; Le Gratiet, 2013; Koziel et al., 2014) due to its computational convenience. Its framework fits well with the multi-sensor geographical information system, since the hierarchy is established based on age and technology of the sensors. In general, newer sensors produce higher fidelity data than the older ones. Most of the computational benefits of the autoregressive co-kriging are lost

when the multi-fidelity data are not observed in a hierarchically nested structure. Multi-sensor geographical information systems are usually observed irregularly in space and are hierarchically non-nested. Recently, Konomi and Karagiannis (2019) proposed a Bayesian augmented hierarchical co-kriging procedure which makes the analysis of partially-nested and/or non-nested structures possible with feasible computational cost by splitting the augmented likelihood into conditionally independent parts. The posterior can now be split into simpler conditionally independent components. Despite this simplification, the method cannot be applied directly in the presence of large data sets. Each conditional component of the likelihood requires evaluation of the determinant as well as inversion of a large co-variance matrix.

Statistical methods for large spatial data-sets have received much attention in the recent past. Many of the most popular techniques rely on low-rank approximation (Banerjee et al., 2008; Cressie and Johannesson, 2008), approximate likelihood methods (Stein et al., 2004; Gramacy and Apley, 2015), covariance tapering methods (Furrer et al., 2006; Kaufman et al., 2008; Du et al., 2009), sparse structures (Lindgren et al., 2011; Nychka et al., 2015; Datta et al., 2016a), multiple-scale approximation (Sang and Huang, 2012; Katzfuss, 2016), and lower dimensional conditional distributions (Vecchia, 1988; Stein et al., 2004; Datta et al., 2016a; Katzfuss and Guinness, 2017). A number of these methods have been generalized to handle large data from multiple sources. For example, Nguyen et al. (2012, 2017) have proposed data fusion techniques based on fixed ranked kriging (Cressie and Johannesson, 2008). The accuracy of this approach relies on the number of basis functions and can only capture large scale variation of the covariance function. When the data-sets are dense, strongly correlated, and the noise effect is sufficiently small, the low rank kriging techniques have difficulty to account for small scale variation (Stein, 2014). More recently, Taylor-Rodriguez et al. (2018) embed NNGP into a spatial factor model and use NNGP to model the resulting independent GP processes. This method is based on the assumption that

data-sets of different sources follow an overlapping structure, which makes it limited for real applications.

In this paper, we propose a new computationally efficient autoregressive co-kriging method based on the nearest neighbor Gaussian process (NNGP), which is called the nearest neighbor Co-kriging Gaussian process (NNCGP). The proposed method is able to address applications for large non-nested and irregular spatial data-sets from different platforms and with varying quality. The method utilizes an approximate imputation procedure based on the knot selection to address large data-sets of non-nested observations. This formulation allows the evaluation of the likelihood and predictions with low computational cost, as well as allows the specification of conditional conjugate priors. Compared to the aforementioned models, it exhibits both computational efficiency and flexibility. This method enables the analysis of high-resolution infrared radiation sounder (HIRS) data-sets gathered daily from two polar orbiting satellite series (POES) of the National Oceanic and Atmospheric Administration (NOAA). We show that the proposed method is both more accurate and computationally more efficient for these type of data-sets. Furthermore, the NNCGP model shows significant improvement in prediction accuracy over the existing NNGP approach, based on our simulation study and the analysis of the real data application.

The layout of the paper is as follows. In Section 2, we introduce a spatial representation of the autoregressive co-kriging model. In Section 3, we introduce our proposed NNCGP as an extension of the existing autoregressive co-kriging model. In Section 4, we design an MCMC approach tailored to the proposed NNCGP model that facilitates parametric and predictive inference. In Section 5, we investigate the performance of the proposed procedure on a toy example. In Section 6, we apply the proposed method for the analysis of NNCGP model on data-sets from two satellites, NOAA-14 and NOAA-15. Finally, we conclude in Section 7.

## 2 Spatial Co-kriging Gaussian Process

Consider  $T$  levels of fidelity spatially observed datasets. Let  $y_t(s)$  denote the output at the spatial location  $s$  at fidelity level  $t = 1, \dots, T$ . Here, the fidelity level index  $t$  runs from the least accurate to the most accurate one. We consider that the observed output  $z_t(s)$  at location  $s$  is contaminated by additive random noise  $\epsilon_t \sim N(0, \tau_t)$  with unknown variance  $\tau_t$ , and  $y_t(s)$  depends on the fidelity level output  $y_{t-1}(s)$  via an autoregressive co-kriging mode. Specifically, we model the observation  $z_t(s)$  as:

$$\begin{aligned} z_t(s) &= y_t(s) + \epsilon_t \\ y_t(s) &= \zeta_{t-1}(s)y_{t-1}(s) + \delta_t(s), \\ \delta_t(s) &= \mathbf{h}_t^T(s)\boldsymbol{\beta}_t + w_t(s), \end{aligned} \tag{2.1}$$

for  $t = 2, \dots, T$ , and  $y_1(s) = \mathbf{h}_1^T(s)\boldsymbol{\beta}_1 + w_1(s)$ . Here,  $\zeta_{t-1}(s)$  and  $\delta_t(s)$  represent the scale and additive discrepancies between systems with fidelity levels  $t$  and  $t - 1$ . Moreover,  $\mathbf{h}_t(\cdot)$  is a basis function,  $\boldsymbol{\beta}_t$  is a vector of coefficients at fidelity level  $t$ . We model, a priori,  $w_t(s)$  as Gaussian processes, mutually independent for different  $t$ ; i.e.  $w_t(\cdot) \sim GP(0, C_t(\cdot, \cdot, \boldsymbol{\theta}_t))$  where  $C_t(\cdot, \cdot, \boldsymbol{\theta}_t)$  is a cross-covariance function with covariance parameters  $\boldsymbol{\theta}_t$  at fidelity level  $t$ . This implies that  $\delta_t(s)$ , given  $\mathbf{h}_t(s)\boldsymbol{\beta}_t$ , is a Gaussian process. The unknown scale discrepancy function  $\zeta_{t-1}(s)$  is modeled as a basis expansion  $\zeta_{t-1}(s|\boldsymbol{\gamma}_{t-1}) = \mathbf{g}_{t-1}(s)^T\boldsymbol{\gamma}_{t-1}$  (usually low degree), where  $\mathbf{g}_t(s)$  is a vector of polynomial bases and  $\{\boldsymbol{\gamma}_{t-1}\}$  is a vector of coefficients for the scale discrepancies, for  $t = 2, \dots, T$ .

The statistical model in (2.1) is different from that based on the co-kriging model of Kennedy and O'Hagan (2000) which is often used in the analysis of computer models because it accounts for a nugget effect. Unlike computer models whose outcome has no random error when computed by deterministic solvers, spatial statistics may involve measurement errors or spatial sources of variation at distances smaller than the sampling interval; hence

the introduction of nugget effect can play an important role. The benefits of considering a nugget effect in the model for spatial data has been noticed by Cressie (1993) and Stein (1999). Gramacy and Lee (2012) argued that the use of a nugget can also mitigate poor fitting when there is deviation from the GP model assumptions. Note that in (2.1),  $y_1, \delta_2, \dots, \delta_T$  are mutually independent. Finally, the Markovian condition  $\text{cov}(y_t(s), y_{t-1}(s')|y_{t-1}(s)) = 0$  is still valid; i.e, there is nothing more to learn about  $y_t(s)$  from  $y_{t-1}(s')$  for any  $s' \neq s$  given that  $y_{t-1}(s)$  is known.

Any valid covariance function  $C_t(\cdot, \cdot | \boldsymbol{\theta}_t)$  can be used to model (Williams and Rasmussen, 2006). A popular choices in spatial statistics, due to its simplicity and effectiveness, is the exponential covariance function Cressie (1993); Stein (1999). For each level of fidelity, we choose a diagonal anisotropic exponential covariance function:  $C_t(s, s' | \boldsymbol{\theta}_t) = \sigma_t^2 \exp\left(-\frac{1}{2} \sum_{i=1}^d \frac{|s_i - s'_i|}{\phi_{t,i}}\right)$ , where  $\boldsymbol{\theta}_t = \{\sigma_t^2, \boldsymbol{\phi}_t\}$ ,  $\sigma_t^2$  is the variance parameter and  $\boldsymbol{\phi}_t = (\phi_{t,1}, \phi_{t,2}, \dots, \phi_{t,d})$  is the anisotropic spatial effect parameter of  $\mathbb{R}^d$  at fidelity level  $t$ .

Let's assume the system is observed at  $n_t$  locations at each fidelity level  $t$ . Let  $\mathbf{S}_t = \{s_{t,1}, \dots, s_{t,n_t}\}$  be the set of  $n_t$  observed locations and  $\mathbf{Z}_t = z_t(\mathbf{S}_t) = \{z_t(s_{t,1}), \dots, z_t(s_{t,n_t})\}$  represent the observed output at fidelity level  $t$ . The joint distribution of the observations at all levels  $\mathbf{Z}_{1:T} = \{\mathbf{Z}_1, \dots, \mathbf{Z}_T\}$  is Gaussian, hence the likelihood  $L(\mathbf{Z}_{1:T} | \boldsymbol{\theta}_{1:T}, \boldsymbol{\beta}_{1:T}, \boldsymbol{\gamma}_{1:T-1}, \tau_{1:T})$  is a multivariate normal density function with mean vector  $\boldsymbol{\mu}$  and covariance matrix  $\boldsymbol{\Lambda}$  that cannot be easily computed. If data are observed in non-nested locations for each fidelity levels, the calculation of the likelihood requires  $\mathcal{O}((\sum_{t=1}^T n_t)^3)$  flops to invert the covariance matrix  $\boldsymbol{\Lambda}$  and additional  $\mathcal{O}((\sum_{t=1}^T n_t)^2)$  memory to store it as explained in Konomi and Karagiannis (2019). Thus the exact evaluation is computationally costly, if not practically impossible, when  $n_t$  is large. For instance, in our application, for each satellite we have  $\sim 10^5$  observations at non-nested locations making the practical implementation impossible.

Nearest-neighbor Gaussian process (NNGP) (Datta et al., 2016a), which uses a latent variable representation, can be used to reduce computational complexity and memory stor-

age. A naive implementation of NNGP in the multi-fidelity setting could possibly ignore certain benefits from the autoregressive structure of model (2.1) leading to inefficient computations. For instance, one could apply NNGP directly to the latent variable representation based on the euclidean distances ignoring the different fidelity levels. However, for a given location and fidelity level  $t$ , the nearest neighbors may be observations that belong in different fidelity level. This may result in poor prediction performances of the high fidelity level, because the nearest neighbors may be observations from lower fidelity. A possible solution which accounts for different level of fidelity is to apply the neighbors based on a dynamic procedure as described in Datta et al. (2016b). The nearest neighbors can be determined based on the dynamic procedure where the increased level of fidelity can be viewed as the time component. However, this procedure adds one more step and the fact that we have a lot of non-overlapping locations at different fidelity levels can complicate computations further. In what follows, we propose an efficient procedure that overcomes the aforesaid issues.

### 3 Nearest Neighbor Co-kriging Gaussian Process

We propose to apply a set of independent NNGP priors at each level of fidelity. Let  $\mathbf{w}_t = w_t(\mathbf{S}_t) = \{w_t(s_{t,1}), \dots, w_t(s_{t,n_t})\}$  denote the vector of the latent process over the observed locations  $\mathbf{S}_t$  at fidelity level  $t$ . Based on the independent assumptions in (2.1), the joint density of  $\mathbf{w}_{1:T}$  can be written as the product of conditional Normal densities:

$$p(\mathbf{w}_{1:T}|\boldsymbol{\theta}_{1:T}) = \prod_{t=1}^T p(\mathbf{w}_t|\boldsymbol{\theta}_t) = \prod_{t=1}^T \prod_{i=1}^{n_t} p(w_t(s_{t,i})|\mathbf{w}_{t,< i}), \quad (3.1)$$

where  $p(\mathbf{w}_t|\boldsymbol{\theta}_t) = N(\mathbf{w}_t|0, \mathbf{C}(\boldsymbol{\theta}_t))$ ,  $\prod_{i=1}^{n_t} p(w_t(s_{t,i})|\mathbf{w}_{t,< i})$  the conditional representation of the joint distribution of  $\mathbf{w}_t$ ,  $\mathbf{w}_{t,< i} = \{w_t(s_{t,1}), w_t(s_{t,2}), \dots, w_t(s_{t,i-1})\}$  for  $2 \leq i \leq n_t$ , and  $\mathbf{w}_{t,< 1} = \emptyset$ . To reduce the computational complexity, we can model each separate component with a nearest neighbor Gaussian Process (NNGP) as in (Datta et al., 2016a). First, we need to specify a multivariate Gaussian distribution over a fixed set of points in the domain, to

which we refer as the *reference set*. For simplicity and computational efficiency, the reference set is chosen to coincide with the set of observed locations  $\mathbf{S}_t$ . As demonstrated in (Datta et al., 2016a), based on the reference set, we can extend this finite-dimensional multivariate normal distribution to a stochastic process over the domain.

Let  $N_t(s_{t,i})$  to be a subset of locations  $\mathbf{S}_{t,< i} = \{s_{t,1}, s_{t,2}, \dots, s_{t,i-1}\}$ .  $N_t(s_{t,i})$  is constructed by choosing at most  $m$  “nearest neighbors” of location  $s_{t,i}$  in  $\mathbf{S}_{t,< i}$ :

$$N_t(s_{t,i}) = \begin{cases} \emptyset & , \text{ for } i = 1, \\ \{s_{t,1}, s_{t,2}, \dots, s_{t,i-1}\} & , \text{ for } 2 \leq i \leq m, \\ m \text{ nearest neighbors among } \{s_{t,1}, s_{t,2}, \dots, s_{t,i-1}\} & , \text{ for } i > m. \end{cases}$$

Given the above specification of nearest neighbors, and its ordering mechanism, the density  $p(\mathbf{w}_t|\boldsymbol{\theta}_t)$  is approximated by  $\tilde{p}(\mathbf{w}_t|\boldsymbol{\theta}_t) = \prod_{i=1}^{n_t} p(w_t(s_{t,i})|\mathbf{w}_{t,N_t(s_{t,i})})$ . It can be shown that  $w_t(s_{t,i})|\mathbf{w}_{t,N_t(s_{t,i})} \sim N(\mathbf{B}_{t,s_{t,i}}\mathbf{w}_{t,N_t(s_{t,i})}, F_{t,s_{t,i}})$ , where  $\mathbf{B}_{t,s_{t,i}} = \mathbf{C}_{s_{t,i}, N_t(s_{t,i})}^T \mathbf{C}_{N_t(s_{t,i})}^{-1}$ ,  $F_{t,s_{t,i}} = \mathbf{C}(s_{t,i}, s_{t,i}) - \mathbf{C}_{s_{t,i}, N_t(s_{t,i})}^T \mathbf{C}_{N_t(s_{t,i})}^{-1} \mathbf{C}_{s_{t,i}, N_t(s_{t,i})}$  is the covariance matrix of  $w_t(s_{t,i})$  and  $\mathbf{w}_{t,N_t(s_{t,i})}$ , and  $\mathbf{C}_{N_t(s_{t,i})}$  is the covariance matrix of  $\mathbf{w}_{t,N_t(s_{t,i})}$ . Thus the nearest neighbor density  $\tilde{p}(\mathbf{w}_t|\boldsymbol{\theta}_t)$  is normal with mean zero and covariance  $\tilde{\mathbf{C}}(\boldsymbol{\theta}_t)$ , where  $\tilde{\mathbf{C}}^{-1}(\boldsymbol{\theta}_t)$  is a sparse matrix with at most  $\frac{1}{2}n_t m(m+1)$  non-zero elements (Appendix A).

With NNGP prior specification for  $\mathbf{w}_t$  and general prior formualtion for  $\boldsymbol{\Theta}_t = (\boldsymbol{\phi}_t, \boldsymbol{\sigma}_t^2, \boldsymbol{\beta}_t, \boldsymbol{\gamma}_{t-1}, \tau_t)$ , the posterior distribution is such as

$$p(\boldsymbol{\Theta}_{1:T}, \mathbf{w}_{1:T} | \mathbf{Z}_{1:T}) \propto \left\{ \prod_{t=1}^T p(\boldsymbol{\Theta}_t) \tilde{p}(\mathbf{w}_t | \boldsymbol{\theta}_t) \right\} L(\mathbf{Z}_{1:T} | \boldsymbol{\theta}_{1:T}, \boldsymbol{\beta}_{1:T}, \boldsymbol{\gamma}_{1:T-1}, \tau_{1:T}, \mathbf{w}_{1:T}) \quad (3.2)$$

while the likelihood kernel is a multivariate normal density with mean  $\boldsymbol{\mu}$  and covariance  $\boldsymbol{\Lambda}$ , which are defined in Appendix B. The covariance matrix  $\boldsymbol{\Lambda}$  is not sparse since the cross covariance in  $\mathbf{S}_{t'} \setminus \mathbf{S}_t$  for  $t' > t$  is not zero. So the likelihood, conditional on the nearest neighbours latent variables, cannot be simplified unless  $\mathbf{S}_{t'} \setminus \mathbf{S}_t = \emptyset$  (or equivalently  $\mathbf{S}_{t'} \subseteq \mathbf{S}_t$ , the observation locations are observed in a nested hierarchical structure). Thus, the direct implementation of NNGP on  $\mathbf{w}_{1:T}$  when observed locations are not fully nested (such that

$\mathbf{S}_t \setminus \mathbf{S}_{t'} = \emptyset$  for  $t > t'$ ) may still lead to infeasible computational complexity.

To overcome the computational issue, we introduce new evaluations of the latent process  $w_t(\cdot)$  for each level. The new evaluations of  $w_t(\cdot)$  are done in such a way that the reference set of level  $t$  is nested to the reference set of level  $t + 1$ . Choosing the reference set in a fully nested structure can factorize the likelihood and the posterior into  $T$  conditional independent parts. Moreover, each of the conditional independent parts of the factorized likelihood has a diagonal covariance matrix similar to NNGP. We call this new computationally efficient procedure the Nearest Neighbor Co-kriging Gaussian Process (NNCGP). The NNCGP utilizes the computational advantages of both the auto-regressive co-kriging model as well as the NNGP. The proposed NNCGP is a well-defined process derived from a parent Co-kriging Gaussian process.

Consider observed data-sets  $\{\mathbf{Z}_t, \mathbf{S}_t\}$ , with the corresponding spatial process vectors and output vectors  $\mathbf{y}_t = y_t(\mathbf{S}_t) = \{y_t(s_{t,1}), \dots, y_t(s_{t,n_t})\}$ . Set  $\mathbf{S}_t^* = \bigcup_{i=t+1}^T \mathbf{S}_i \setminus \mathbf{S}_t = \{s_{t,1}^*, \dots, s_{t,n_t^*}^*\}$  as additional reference set of fidelity level  $t$ , which contains the observed locations that are not in  $t^{th}$  level but in higher fidelity levels, and denote  $\mathbf{w}_t^* = \{w_t(s_{t,1}^*), \dots, w_t(s_{t,n_t^*}^*)\}$  as the latent interpolants with corresponding  $\mathbf{y}_t^*$ . Let  $\tilde{\mathbf{w}}_t = \mathbf{w}_t^* \cup \mathbf{w}_t$ ,  $\tilde{\mathbf{y}}_t = y_t(\mathbf{S}_t^*) \cup y_t(\mathbf{S}_t)$ ,  $\tilde{\mathbf{S}}_t = \mathbf{S}_t^* \cup \mathbf{S}_t$ , and  $\tilde{n}_t = n_t + n_t^*$ , thus the complete observed locations  $\tilde{\mathbf{S}}_t$  and  $\mathbf{S}_{t'}$  have a nested hierarchical structure with  $\mathbf{S}_{t'} \subseteq \tilde{\mathbf{S}}_t$  when  $t' \geq t$ . By sequentially adding  $\mathbf{w}_t^*$  to each level, we can construct a fully nested hierarchical model. To better understand the proposed procedure, we give a directed acyclic graphs (DAG) representation of a toy example with two fidelity levels in Figure 1.

Using the Markovian property of the co-kriging model, the joint likelihood can be now factorized as a product of likelihoods from different fidelity levels conditional on augmented

### Graphical representation of NNCGP

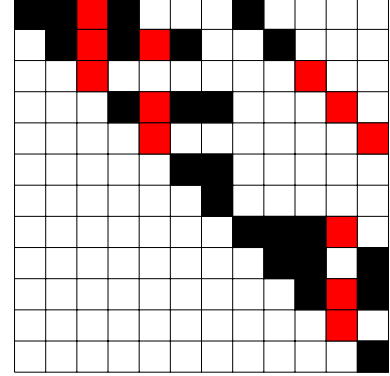
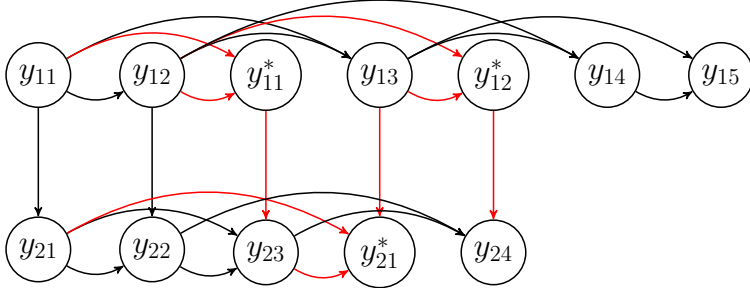


Figure 1: Toy examples of the NNCGP for two fidelity levels ( $T=2$ ) with  $n_1 = 5$ ,  $n_2 = 4$ ,  $n_1^* = 2$ . Left: directed acyclic graphical representation of the noiseless part of the NNCGP model. Right: covariance matrix sparsity of the model (white rectangle represent zero cross-covariance).

latent interpolants, i.e.:

$$\begin{aligned}
 L(\mathbf{Z}_{1:T}|\cdot) &= p(\mathbf{Z}_1|\mathbf{w}_1, \boldsymbol{\beta}_1, \tau_1) \prod_{t=2}^T p(\mathbf{Z}_t|\mathbf{w}_t, \boldsymbol{\beta}_t, y_{t-1}(\mathbf{S}_t), \boldsymbol{\gamma}_{t-1}, \tau_t) \\
 &= N(\mathbf{Z}_1|\mathbf{h}_1(\mathbf{S}_1)\boldsymbol{\beta}_1 + \mathbf{w}_1, \tau_1 \mathbf{I}) \prod_{t=2}^T N(\mathbf{Z}_t|\zeta_{t-1}(\mathbf{S}_t) \circ y_{t-1}(\mathbf{S}_t) + \delta_t(\mathbf{S}_t), \tau_t \mathbf{I}),
 \end{aligned} \quad (3.3)$$

where  $\circ$  is the Hadamard production symbol and  $y_{t-1}(\mathbf{S}_t) \subset \tilde{\mathbf{y}}_{t-1}$ . Based on the NNNGP prior on the  $\mathbf{w}_{1:T}$  described above, we can write the joint prior distribution of  $\tilde{\mathbf{w}}_{1:T}$  as:

$$\begin{aligned}
 p(\tilde{\mathbf{w}}_{1:T}|\boldsymbol{\theta}_{1:T}) &= p(\mathbf{w}_1^*|\mathbf{w}_{1:T}, \boldsymbol{\theta}_{1:T})p(\mathbf{w}_{1:T}|\boldsymbol{\theta}_{1:T}), \\
 &= \prod_{t=1}^T p(\mathbf{w}_t^*|\mathbf{w}_t, \boldsymbol{\theta}_t)p(\mathbf{w}_t|\boldsymbol{\theta}_t).
 \end{aligned} \quad (3.4)$$

Given the above representation of the likelihood and prior, the joint posterior density function of NNCGP for a  $T$  level system is:

$$\begin{aligned}
 p(\boldsymbol{\Theta}_{1:T}, \tilde{\mathbf{w}}_{1:T}|\mathbf{Z}_{1:T}) &\propto p(\boldsymbol{\Theta}_1)\tilde{p}(\mathbf{w}_1|\boldsymbol{\theta}_1)\tilde{p}(\mathbf{w}_1^*|\mathbf{w}_1, \boldsymbol{\theta}_1)N(\mathbf{Z}_1|\mathbf{h}_1(\mathbf{S}_1)\boldsymbol{\beta}_1 + \mathbf{w}_1, \tau_1 \mathbf{I}) \\
 &\times \prod_{t=2}^T \{p(\boldsymbol{\Theta}_t)\tilde{p}(\mathbf{w}_t|\boldsymbol{\theta}_t)\tilde{p}(\mathbf{w}_t^*|\mathbf{w}_t, \boldsymbol{\theta}_t)N(\mathbf{Z}_t|\zeta_{t-1}(\mathbf{S}_t) \circ y_{t-1}(\mathbf{S}_t) + \delta_t(\mathbf{S}_t), \tau_t \mathbf{I})\}.
 \end{aligned} \quad (3.5)$$

The computational complexity of implementing NNCGP model is dominated by the evaluation and storage of  $T$  sparse matrices  $(\tilde{\mathbf{C}}_1^{-1}(\boldsymbol{\theta}_1), \dots, \tilde{\mathbf{C}}_T^{-1}(\boldsymbol{\theta}_T))$ . Thus, the joint posterior

distribution of NNCGP model can be calculated using  $\mathcal{O}(\sum_{t=1}^T \tilde{n}_t m^3)$  flops and the storage needs  $\mathcal{O}(\sum_{t=1}^T \tilde{n}_t m^2)$  dynamic memory. Introducing  $\mathbf{w}_{1:T}^*$  reduces the computational complexity as well as enabling the specification of semi-conjugate priors for  $(\boldsymbol{\sigma}_t^2, \boldsymbol{\beta}_t, \boldsymbol{\gamma}_{t-1}, \tau_t)$  which facilitates tractability of posterior marginals and conditionals, as we explain below.

## 4 Bayesian Inference

In this section, we present the MCMC sampler for the inference of parameters  $\boldsymbol{\Theta}_{1:T}$  for a  $T$  level NNCGP with observations  $\mathbf{Z}_{1:T}$  and spatial location input sets  $\mathbf{S}_{1:T}$ . We also present the prediction procedure for output  $\mathbf{Z}_t(s_p)$  at an unobserved location  $s_p$  for any specified fidelity level  $t$ .

NNCGP model representation allows us to construct an efficient MCMC sampler to facilitate parameter and prediction inference. Imputation of the latent interpolants  $\mathbf{w}_t^*$  allows the conditional independency (3.3), as well as it is particularly useful when a certain fidelity level has missing observations. Since the components of  $\mathbf{w}_t^* | \mathbf{w}_t$  are independent, we can update  $\mathbf{w}_t^*$  individually. For locations  $s_u \in \mathbf{S}_t^*$ , the full conditional posterior distribution of  $w_t(s_u)$  is  $N(F_{t,s_u}^{-1} \mathbf{B}_{t,s_u} \mathbf{w}_{t,N_t(s_u)}, F_{t,s_u})$ , for  $t = 1, 2, \dots, T-1$ . Where  $\mathbf{B}_{t,s_u} = \mathbf{C}_{s_u, N_t(s_u)}^T \mathbf{C}_{N_t(s_u)}^{-1}$  and  $F_{t,s_u} = \mathbf{C}(s_u, s_u) - \mathbf{C}_{s_u, N_t(s_u)}^T \mathbf{C}_{N_t(s_u)}^{-1} \mathbf{C}_{s_u, N_t(s_u)}$ ,  $\mathbf{C}_{s_u, N_t(s_u)}$  are the covariance matrices of  $w_t(s_u)$  and  $\mathbf{w}_{t,N_t(s_u)}$ , and  $\mathbf{C}_{N_t(s_u)}$  is the covariance matrix of  $\mathbf{w}_{t,N_t(s_u)}$ .

The introduction of the latent interpolant  $\mathbf{w}_{t-1}^*$  provides the full conditional posterior distribution of spatial random process  $\mathbf{w}_t$ :

$$\begin{aligned} w_t(s_u) | \boldsymbol{\beta}_t, \boldsymbol{\theta}_t, \tau_t, \mathbf{Z}_t, \tilde{\mathbf{y}}_{t-1}, \boldsymbol{\gamma}_{t-1} &\sim N(V_{\mathbf{w}_t}(s_u) \mu_{\mathbf{w}_t}(s_u), V_{\mathbf{w}_t}(s_u)),, \\ V_{\mathbf{w}_t}(s_u) &= (F_{t,s_u}^{-1} + \tau_t^{-2})^{-1}, \\ \mu_{\mathbf{w}_t}(s_u) &= \tau_t^{-2} [z_t(s_u) - \mathbf{h}_t^T(s_u) \boldsymbol{\beta}_t - \zeta_{t-1}(s_u) y_{t-1}(s_u)] + F_{t,s_u}^{-1} \mathbf{B}_{t,s_u} \mathbf{w}_{t,N_t(s_u)}, \end{aligned} \quad (4.1)$$

for  $t = 2, \dots, T$ ,  $s_u \in \mathbf{S}_t$ . The full conditional distribution of  $\mathbf{w}_1$  is similar to the univariate case of full conditional distribution of spatial process Datta et al. (2016a), C.1 of the

Appendix.

To take full advantage of the posterior representation in (3.5), we chose independent prior distributions for parameters at different levels such as:

$$p(\boldsymbol{\Theta}_{1:T}) = \prod_{t=1}^T p(\sigma_t) p(\boldsymbol{\phi}_t) p(\boldsymbol{\beta}_t) p(\tau_t) p(\boldsymbol{\gamma}_{t-1}). \quad (4.2)$$

The above prior representation coupled with (3.5) results into  $T$  separate conditional parts for the posterior. To facilitate further computations, we assign conditional conjugate priors:  $\sigma_t^2 \sim IG(a_t, b_t)$ ,  $\boldsymbol{\beta}_t \sim N(\boldsymbol{\mu}_{\boldsymbol{\beta}_t}, \mathbf{V}_{\boldsymbol{\beta}_t})$ ,  $\tau_t^2 \sim IG(c_t, d_t)$ ,  $t = 1, 2, \dots, T$ ;  $\boldsymbol{\gamma}_{t-1} \sim N(\mu_{\boldsymbol{\gamma}_{t-1}}, V_{\boldsymbol{\gamma}_{t-1}})$ ,  $t = 2, 3, \dots, T$ , which lead to standard full conditional posteriors

$$\begin{aligned} \boldsymbol{\beta}_t | \mathbf{w}_t, \tilde{\mathbf{y}}_{t-1}, \boldsymbol{\gamma}_{t-1}, \tau_t, \mathbf{Z}_t &\sim N(\mathbf{V}_{\boldsymbol{\beta}_t}^* \boldsymbol{\mu}_{\boldsymbol{\beta}_t}^*, \mathbf{V}_{\boldsymbol{\beta}_t}^*), \\ \boldsymbol{\gamma}_t | \tilde{\mathbf{y}}_t, \boldsymbol{\beta}_{t+1}, \tau_{t+1}, \mathbf{Z}_{t+1} &\sim N(\mathbf{V}_{\boldsymbol{\gamma}_t}^* \boldsymbol{\mu}_{\boldsymbol{\gamma}_t}^*, \mathbf{V}_{\boldsymbol{\gamma}_t}^*), \\ \sigma_t^2 | \tilde{\mathbf{w}}_t, \boldsymbol{\phi}_t &\sim IG(a_{\sigma_t}^*, b_{\sigma_t}^*), \\ \tau_t | \boldsymbol{\beta}_t, \mathbf{w}_t, \tilde{\mathbf{y}}_{t-1}, \mathbf{Z}_t, \boldsymbol{\gamma}_{t-1} &\sim IG(a_{\tau_t}, b_{\tau_t}), \end{aligned} \quad (4.3)$$

where the parameters are specified in C.2-C.6 of the Appendix. For the range parameter  $p(\phi_{t,j})$ , we choose bounded prior  $p(\phi_{t,j}) \sim U(0, l_{t,j})$  to avoid numerical instabilities, where  $l_{t,j}$  is defined from the researcher and is usually associated with the maximum distance in the  $j^{th}$  direction. The conditional posterior distribution for  $\boldsymbol{\phi}_t$  in NNCGP model is

$$p(\boldsymbol{\phi}_t | \tilde{\mathbf{w}}_t, \sigma_t^2) \propto p(\boldsymbol{\phi}_t) |\tilde{\mathbf{C}}(\boldsymbol{\theta}_t)|^{-1/2} \exp \left\{ -\frac{1}{2} \tilde{\mathbf{w}}_t^T \tilde{\mathbf{C}}^{-1}(\boldsymbol{\theta}_t) \tilde{\mathbf{w}}_t \right\}, \quad (4.4)$$

where  $\boldsymbol{\phi}_t$  appears in the sparse cross covariance matrix  $\tilde{\mathbf{C}}(\boldsymbol{\theta}_t)$  and it cannot be sampled directly. The Metropolis-Hastings algorithm (Hastings, 1970) can be used to update  $\boldsymbol{\phi}_t$  in the full conditional distribution. Based on the above prior specification and the resulting conditional posterior distributions, the Bayesian inference can be derived in parallel for each fidelity level. In this case, if parallel computing is available, the computational complexity of the approach can be reduced up to  $\mathcal{O}(\tilde{n}_1 m^3)$ .

For a new input location  $s_p \notin \tilde{\mathbf{S}}_t$ , the prediction process is to generate  $z_t(s_p)$  based on its predictive distribution. Subsequently, we generate  $w_{t'}(s_p)$  independently for each level from sampler  $w_{t'}(s_p) \sim N(V_{t',s_p}\mu_{t',s_p}, V_{t',s_p})$  for  $t' = 1, \dots, t$ ; where  $V_{t',s_p}$ ,  $\mu_{t',s_p}$  are specified in (C.7), while  $y_{t'}(s_p)$  are generated by  $y_{t'}(s_p) = \zeta_{t'-1}(s_p)y_{t'-1}(s_p) + \mathbf{h}_{t'}(s_p)\boldsymbol{\beta}_{t'} + w_{t'}(s_p)$ . The  $z_t(s_p)$  is generated by the MCMC sampler  $z_t(s_p)| \cdot \sim N(y_t(s_p), \tau_t)$ .

## 5 Synthetic Data Example

This section conducts a simulation study to evaluate the performance of the proposed NNCGP model in comparison with the NNGP model using the highest fidelity level data only (denoted as single level NNGP model) and using both fidelity level data-sets combined as a single data-set (denoted as combined NNGP model). Details about the measure metrics used for the comparison can be found in Appendix D. Simulations were performed in MATLAB R2018a, on a computer with specifications (intelR i7-3770 3.4GHz Processor, RAM 8.00GB, MS Windows 64bit).

We consider a two-fidelity level system, in a two dimensional unit square domain, parameterized as an auto-regressive co-kriging Gaussian process specified in (2.1). For simplicity, the mean of  $y_1(s)$ , the mean of the additive discrepancy  $\delta_2(s)$ , and the scalar discrepancy  $\zeta_1(s)$  are assumed constant. Also the covariance function of  $y_1(s)$  and  $\delta_2(s)$  is assumed exponential. The true values of the model parameters are listed in the first column of Table 1. Based on the above statistical model, we generated 5,000 observations for each fidelity level  $\mathbf{Z}_1$  and  $\mathbf{Z}_2$  at randomly selected locations  $\mathbf{S}_1$  and  $\mathbf{S}_2$  such that  $\mathbf{S}_1 \cap \mathbf{S}_2 = \emptyset$ . The 10,000 generated datasets are shown in Figure 2(a-c). To assess predictive performance, we randomly select two small square regions as testing dataset in the high fidelity level Figure 2b.

For the Bayesian inference of NNCGP, on the unknown parameters  $\beta_1$ ,  $\beta_2$  and  $\gamma_1$  we assign independent normal prior distributions with zero mean and large variances. Also, we use inverse Gamma priors for the spatial and noise variances  $\sigma_t^2 \sim IG(2, 1)$ ,  $\tau_t^2 \sim IG(2, 1)$ , the

range correlation parameters  $\phi_1$  and  $\phi_2$  have each a uniform prior  $U(0, 100)$ . We use similar non-informative priors for the single level NNGP model as well as the combined NNGP. For all three models, we run the Markov chain Monte Carlo (MCMC) sample described in Section 4 with 35,000 iterations where the first 5,000 iterations are discarded as a burn-in. The convergence of the MCMC sampler was diagnosed from the individual trace plots.

In Table 1, we report the Monte Carlo estimates of the posterior means and the associated 95% marginal credible intervals of the unknown parameters using the three different NNGP based procedures with  $m = 10$ . The true values of the parameters are successfully included in the 95% marginal credible intervals. The introduction of latent interpolants may have causes a small over estimation of  $\tau_2$ . However, the true values of the nugget variances are successfully captured in the 95% marginal credible intervals. The uncertainty in the parameter estimations can be improved with a semi-nested or nested structure between the observed locations of the fidelity levels, as shown for the auto-regressive co-kriging model in Konomi and Karagiannis (2019).

In Table 2, we report standard performance measures (defined in the Appendix D) for the proposed NNCGP, single level NNGP, and combined levels NNGP with  $m = 10$  number of neighbours. All performance measures indicate that NNCGP has better predictive ability than single level NNGP and combined NNGP. NNCGP produces significantly smaller PD and Deviance information criterion (DIC) than the single level NNGP and combined NNGP which suggests that NNCGP provides a better fit when complexity is considered. The root mean square prediction error (RMSPE) produced by NNCGP is approximately 40 - 50% smaller than that of single level NNGP and 20 - 30% smaller than that of combined NNGP. The Nash-Sutcliffe model efficiency coefficient (NSME) of NNCGP is closer to 1 than that of both other methods, which suggests that NNCGP provides a substantial improvement in the prediction.

Figure 2 provide the synthetic observations and the prediction plots from NNCGP, single

	True	Model					
		Single level NNGP		Combined NNGP		NNCGP	
$\beta_1$	10	10.82	(9.84, 11.27)	10.15	(9.57, 10.71)	9.71	(9.36, 10.16)
$\beta_2$	1	-	-	-	-	0.87	(0.39, 1.36)
$\sigma_1^2$	4	3.79	(2.97, 5.19)	4.89	(3.65, 6.27)	3.51	(2.71, 4.52)
$\sigma_2^2$	1	-	-	-	-	1.05	(0.18, 2.31)
$1/\phi_1$	10	13.29	(9.33, 17.51)	8.75	(6.49, 11.94)	10.77	(8.07, 13.91)
$1/\phi_2$	10	-	-	-	-	12.61	(3.93, 24.07)
$\gamma_1$	1	-	-	-	-	0.995	(0.983, 1.051)
$\tau_1^2$	0.1	0.138	(0.115, 0.183)	0.478	(0.451, 0.508)	0.125	(0.097, 0.148)
$\tau_2^2$	0.05	-	-	-	-	0.158	(0.041, 0.232)
$m$	10	-	-	-	-	-	-

Table 1: The unknown parameters are in the 1st column; their true values in the 2nd column; their Bayesian point estimates and marginal credible intervals for the single level NNGP, combined NNGP and NNCGP models are in the 3rd, 4th and 5th columns. The level 2 data set in single level NNGP model, the level 1 and level 2 combined data set in combined NNGP model are treated as following one level system , and the estimated parameters of these data sets by single level NNGP and combined NNGP models are also treated as level 1 parameters.

level NNGP and combined NNGP. In Figures 2, we observe that for the testing regions the NNCGP has more accurately captured the roughness and sharp changes in the response surface while it also provides better presentation of the patterns in prediction surface. Applying NNGP directly in the high fidelity level data-set provides a smoother prediction surface due to the lack of the information from low fidelity level data-set; while it fails to produce reliable predictions at the blank regions. Applying NNGP in the combined data-set from both high and low fidelity levels (combined NNGP) also provides an unreliable prediction surface that is similar to the observations in low level regions. Modeling the scalar and additive discrepancies between different levels correctly helps in getting better predictions. Moreover, NNCGP has produced a CVG closer to 0.95 and a 95% ALCI smaller than that of single level NNGP and combined NNGP (Table 1); this indicates that NNCGP produces more accurate predictions with a higher probability to cover true values with narrower credible intervals.

To test the sensitivity performance of the proposed NNCGP methods with the num-

	Model		
	Single level NNGP	Combined NNGP	NNCGP
RMSPE	2.1325	1.5202	1.0987
NSME	-1.1349	0.0888	0.5108
CVG(95%)	0.8216	0.7136	0.9573
ALCI(95%)	5.2024	3.0856	3.2265
PD	12706	5883	2544
DIC	18136	9659	5551
Time(Hour)	1.4	2.9	4.1

Table 2: Performance measures for the predictive ability of the NNCGP model, single level NNGP model and combined NNGP model. (Definitions are given in the supplementary material)

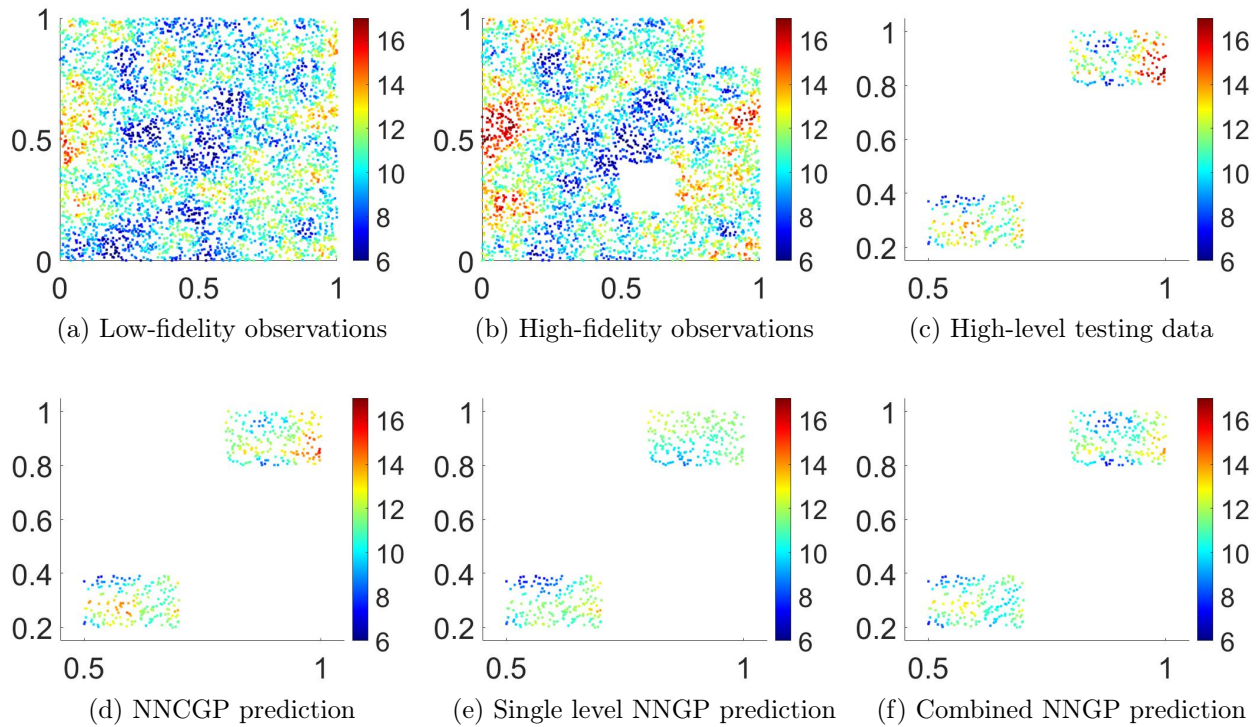


Figure 2: Non-nested structure observations with two fidelity level structure. White boxes indicate the testing regions. Original testing data (c) along with predictions of the high fidelity level data-set by the (d) multifidelity Nearest Neighbor Co-Kriging Gaussian Process (NNCGP), (e) single level nearest neighbor Gaussian process (NNGP), (f) the combined nearest neighbor Gaussian process (NNGP) under the non-nested structure.

ber of neighbors  $m$ , we compare the RMSPEs of the three different methods for  $m = 1, 2, 3, 4, 5, 10, 15$ , and  $20$  in Figure 3(a). We use the same prior specifications as well as computational strategies as above. In terms of the prediction accuracy, the NNCGP outperforms both the single level NNGP and the combined levels NNGP for all  $m$ . The decrease of the RMSPE is smaller as  $m$  become greater than  $10$ . The computational time of NNCGP is slower than single level NNGP and combined levels NNGP (Figure 3(b)). The NNCGP uses data from both levels and also expand the reference set to ensure its nested structure for different levels. The single NNGP model only uses data from the higher fidelity level. The combined levels NNGP uses the same dataset as the NNCGP. However, the reference set of the combined NNGP is equal to the reference set of the first fidelity level of NNCGP. It is worth mentioning that the computational speed of the proposed NNCGP can be improved significantly if parallel computing is available, as explained in Section 4. The computational speed of the parallel version can approximate the computational time of the combined levels NNGP. Moreover, if the observation locations are nested or semi-nested the computational complexity of the NNCGP can be further reduced since  $\tilde{n}_1 < (n_1 + n_2)$ .

## 6 Application: Intercalibrating Satellite Observations

Satellite soundings have been providing measurements of the Earth’s atmosphere, oceans, land, and ice since the 1970s to support the study of global climate system dynamics. Long term observations from past and current environmental satellites are widely used in developing climate data records (CDR) (National Research Council, 2004). We examine here one instrument in particular, the high-resolution infrared radiation sounder (HIRS) instrument that has been taking measurements since 1978 on board the National Oceanic and Atmospheric Administration (NOAA) polar orbiting satellite series (POES) and the meteorological operational satellite program (Metop) series operated by the European Organization for the Exploitation of Meteorological Satellites (EUMETSAT). This series of more than a dozen

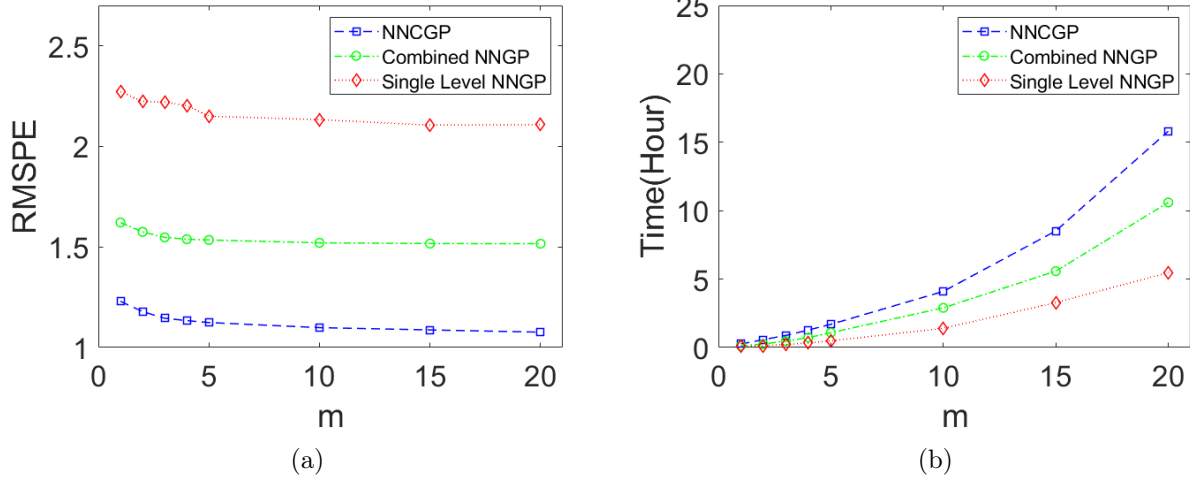


Figure 3: Number of nearest neighbor sensitive analysis: a) Root mean square prediction error(RMSPE) and b) Running time, by NNGP model, single level NNGP model and combined NNGP model for a range of  $m$  for two fidelity level non-nested design synthetic data analysis.

satellites currently constitutes over 40 years of HIRS observations, and this unique longevity is valuable to characterize climatological trends. Examples of essential climate variables derived from HIRS measurements include long-term records of temperature and humidity profiles (Shi et al., 2016; Matthews and Shi, 2019).

HIRS mission objectives include observations of atmospheric temperature, water vapor, specific humidity, sea surface temperature, cloud cover, and total column ozone. The HIRS instrument is comprised of twenty channels, including twelve longwave channels, seven short-wave channels, and one visible channel. Among the longwave channels, Channels 1 to 7 are in the carbon dioxide (CO<sub>2</sub>) absorption band to measure atmospheric temperatures from near-surface to stratosphere, Channel 8 is a window channel for surface temperature observation and cloud detection, Channel 9 is an ozone channel, and Channels 10–12 are for water vapor signals at the near-surface, mid-troposphere, and upper troposphere, respectively. There have been several versions of the instruments where there is a notable change in spatial resolution. In particular, for the HIRS/2 instrument, with observations from the late 1970s

to mid-2007, the spatial footprint is approximately 20 km. HIRS/3, with observations from 1998 to mid-2014, has a spatial footprint of approximately 18 km. The currently operational version, HIRS/4, improved the spatial resolution to approximately 10 km at nadir with observations beginning in 2005. The data-set being considered in this study is limb-corrected HIRS swath data as brightness temperatures (Jackson et al., 2003). The data is stored as daily files, where each daily file records approximately 120,000 geolocated observations. The current archive includes data from NOAA-5 through NOAA-17 along with Metop-02, covering the time period of 1978-2017. In all, this data archive is more than 2 TB, with an average daily file size of about 82 MB.

The HIRS data record faces some common challenges when developing CDRs from the time series. Specifically, there are consistency and accuracy issues due to degradation of sensors and intersatellite discrepancies. Furthermore, there is missing information caused by atmospheric conditions such as thick cloud cover. As early as 1991, to address some of these challenges, the co-kriging technique has been applied to remotely sensed data-sets (Bhatti et al., 1991). As an improvement to these techniques, we consider using the NNGP model as a method for intersatellite calibration, data imputation, and data prediction.

We examine HIRS Channel 5 observations from a single day, March 1, 2001, as illustrated in Figure 4. On this day we may exploit a period of temporal overlap in the NOAA POES series where two satellites captured measurements: NOAA-14 and NOAA-15. The HIRS sensors on these two satellites have similar design patterns, which allow us to ignore the spectral and spatial footprint differences. NOAA-14 became operational in December 1994 while NOAA-15 became operational in October 1998. Given the sensor age difference, it is reasonable to consider that the instruments on-board NOAA-15 are in better condition than those of NOAA-14. Therefore, we treat observations from NOAA-14 as a data-set of low fidelity level, and those from NOAA-15 as a data-set of high fidelity level. A small region from observations of NOAA-15 is treated as testing data, and the rest of NOAA-15 is treated

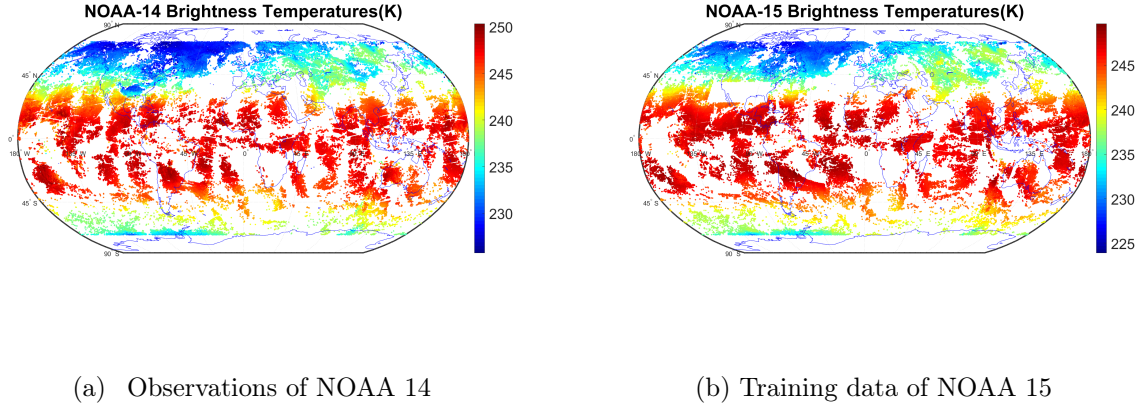


Figure 4: NOAA-14 Brightness Temperatures observation data-set, NOAA-15 Brightness Temperatures training data-set for Channel 5 on March 1, 2001.

as training data.

We model our data based on the two-fidelity level NNCGP model as described in Section 3 & 4. We consider a linear model for the mean of the Gaussian processes, in  $y_1(\cdot)$  and  $\delta_2(\cdot)$ , with linear basis function representation  $\mathbf{h}(s_t)\}$  and coefficients  $\boldsymbol{\beta}_t = \{\beta_{0,t}, \beta_{1,t}, \beta_{2,t}\}^T$ . We consider the scalar discrepancy  $\zeta(s)$  to be unknown constant and equal to  $\gamma$ . The number of nearest neighbors  $m$  is set to 10, and the spatial process  $\mathbf{w}_t$  is consider to have a diagonal anisotropic exponential covariance function as described in Section 3.

We assign independent normal distribution priors with zero mean and large variances for  $\beta_{0,t}, \beta_{1,t}, \beta_{2,t}$  and  $\gamma$ . We assign independent uniform prior distributions  $U(0, 1000)$  to the range correlation parameters  $(\phi_{t,1}, \phi_{t,2})$  for  $t = 1, 2$ . Also, we assign independent  $IG(2, 1)$  prior distributions for the variance parameters  $\sigma_t^2$  and  $\tau_t^2$ . For the Bayesian inference of the NNCGP, we run the MCMC sampler described in Section 4 with of 35,000 iterations where the first 5,000 iterations are discarded as a burn-in.

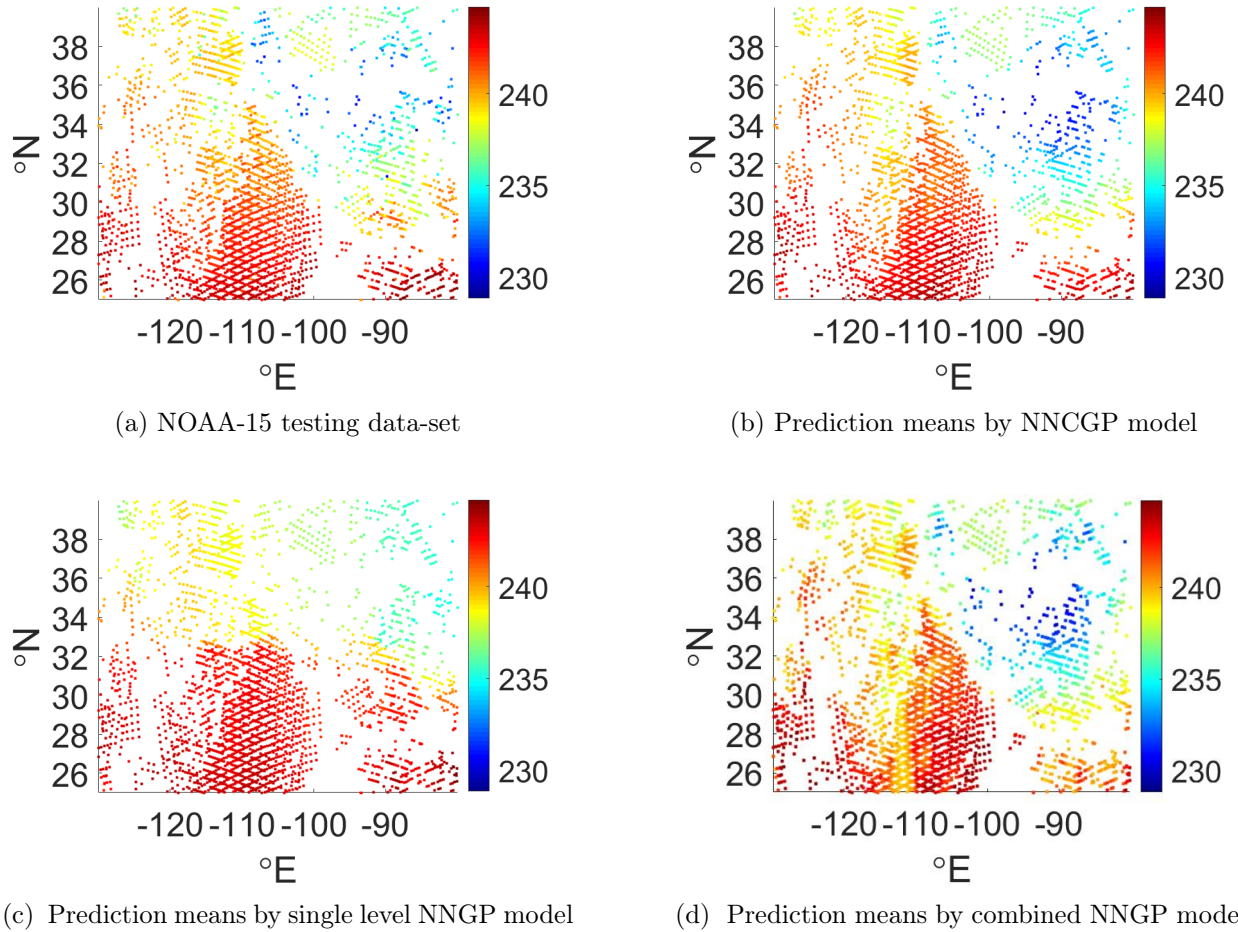


Figure 5: Predictions of NOAA-15 Brightness Temperatures(K) testing data-set by NNCGP, single level NNGP and combined NNGP under fully non-nested experimental design.

	Model		
	NNCGP	Single level NNGP	Combined NNGP
RMSPE	1.2044	1.8153	1.6772
NSME	0.8439	0.5499	0.6726
CVG(95%)	0.9255	0.8350	0.9197
ALCI(95%)	3.094	4.214	5.778
Time(Hour)	38	20	32

Table 3: NOAA 14 and NOAA 15 HIRS instrument data analysis.

The prediction performance metrics of the three different methods are given in Table 3. Compared to the single level NNGP model and combined NNGP model, the NNCGP model

produced a 30% smaller RMSPE and its NSME is closer to 1. The NNCGP also produced larger CVG and smaller ALCI than the single level NNGP model and combined NNGP model. The result suggests that the NNCGP model has a substantial improvement in terms of predictive accuracy in real data analysis too. From the prediction plots (Figure 5) of the testing data of NOAA-15, we can observe that NNCGP model is more capable of capturing the pattern of the testing data than single level NNGP model and combined NNGP model. This is reasonable because the observations from NOAA-14 have provided information of the testing region, and comparing to combined NNGP model, the NNCGP model is capable of modeling the discrepancy of observations from different satellites. In the fully non-nested structure, the computational complexity of the single level NNGP model is  $\mathcal{O}(n_2 m^3)$  and of NNCGP model is  $\mathcal{O}((n_1 + n_2)m^3)$ ; this is consistent with the running times of the models shown in Table 3. Technically, the significant improvement of the prediction accuracy by NNCGP model is important, while the climate variables are very sensitive to the input values. We must emphasize that the variable of interest is the brightness temperature. The baseline observations of the brightness temperature are used as input for so-called remote sensing retrieval algorithms wherein thematic climate variables (e.g. precipitation rates, cloud cover, surface temperature, etc.) are derived. These retrieval algorithms are typically highly nonlinear, so a small change in the input brightness temperature value can have a large impact on derived climate variables. Thus, although the computation by the NNCGP model is costly comparing to the single level NNGP model, it is still worthy to consider applying the NNCGP model in the real data analysis.

We applied the NNCGP model for gap-filling predictions based upon a discrete global grid. We choose to use  $1^\circ$  latitude by  $1.25^\circ$  longitude ( $1^\circ \times 1.25^\circ$ ) pixels as grids with global spatial coverage from  $-70^\circ$  to  $70^\circ$ N. By applying the NNCGP model, we predict gridded NOAA-15 brightness temperature data on the center of the grids, based on the NOAA-14 and NOAA-15 swath-based spatial support. The prediction plot (Figure 6) illustrates the

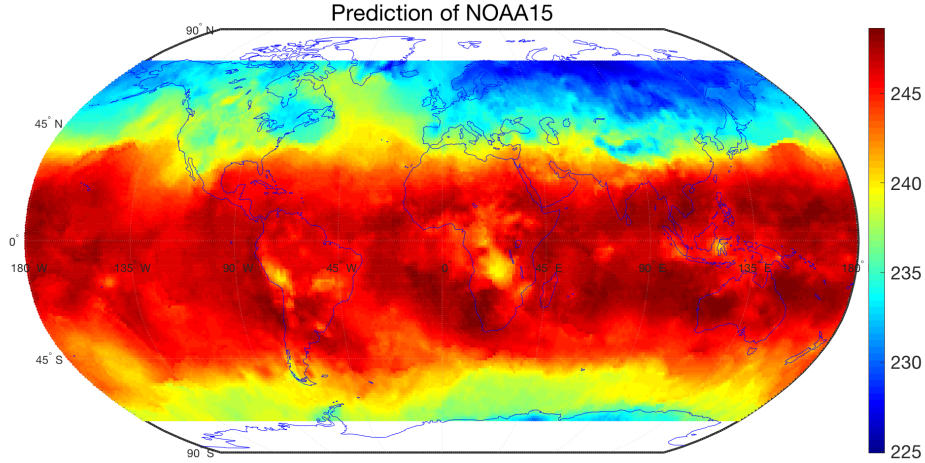


Figure 6: The global prediction plot of NOAA 15

ability of the NNCGP model to handle large irregularly spaced data-sets and produce a gap-filled composite gridded data-set.

## 7 Summary and Conclusions

In this manuscript, we have proposed a new computationally efficient Nearest Neighbor Autoregressive Co-Kriging Gaussian process (NNCGP) method for the analysis of large irregularly spaced and multi-fidelity spatial data. The proposed NNCGP method extends the scope of the classical auto-regressive co-kriging models (Kennedy and O'Hagan, 2000; Konomi and Karagiannis, 2019) to deal with large data-sets. A direct implementation of the nearest neighbor Gaussian processes (NNGP) into the autoregressive co-kriging model is not practically feasible due to the difficulty of the reference set selection as well as the complexity of the covariance function. To deal with this complexity, we use NNGP on the latent variables of each level in the classical auto-regressive co-kriging model where the neighbors are simply defined within each level. However, when the observed locations are hierarchically non-nested, the likelihood does not simplify; this makes the computational complexity of this

approach infeasible. To overcome this issue, we augment the latent variables such that they can form a suitable nested structure. The augmentation of the latent variables facilitates the computation of the likelihood of NNCGP. This is because it enables the factorisation of the likelihood into terms involving smaller covariance matrices and gains the computational efficiency of the nearest neighbors within each level. The proposed method is at most computationally linear in the total number of all spatial locations of all fidelity levels. As we have shown in the paper, computations are faster when the data-sets are observations partially at the same locations for each level. Moreover, the nested design of the reference sets allows the assignment of the semi-conjugate priors for the majority of the parameters. Based on these specifications, we develop efficient and independent MCMC block updates for Bayesian inference. As in the original NNGP paper (Datta et al., 2016a) our results indicate that inference is very robust with respect to values of neighbors.

We compared the proposed NNCGP with NNGP in the single level highest-fidelity in a simulation study and a real data application of intersatellite calibration. We observed that NNCGP was able to improve the accuracy of the prediction for the HIRS brightness temperatures from the NOAA-15 polar-orbiting satellite by incorporating information from an older version of the same HIRS sensor onboard the polar orbiting satellite NOAA-14. The proposed methodology can be used for a variety of large multi-fidelity level data-sets in remote sensing with overlapping similar design patterns. Moreover, the proposed methodology can be used in a wide range of applications in physical science and engineering when multiple computer models with large simulation runs are available.

Several extensions of the proposed NNCGP can be pursued in future work. A possible extension is to speed up our inferential method with a reference or conjugate NNCGP based on ideas given in (Finley et al., 2019). Another possible extension of the proposed model would be to the multivariate settings by using ideas from the parallel partial autoregressive co-kriging (Ma et al., 2019). Moreover, the proposed model can be extended to spatial-

temporal settings with discretized time steps, as both autoregressive structure and the NNGP approach are capable of incorporating temporal dependence.

## 8 Funding acknowledgments

Matthews was supported by National Oceanic and Atmospheric Administration (NOAA) through the Cooperative Institute for Climate and Satellites - North Carolina under Cooperative Agreement NA14NES432003 and the Cooperative Institute for Satellite Earth System Studies under Cooperative Agreement NA19NES4320002.

## References

Aboufirassi, M. and Mariño, M. A. (1984), “Cokriging of aquifer transmissivities from field measurements of transmissivity and specific capacity,” *Journal of the International Association for Mathematical Geology*, 16, 19–35.

Banerjee, S., Gelfand, A. E., Finley, A. O., and Sang, H. (2008), “Gaussian predictive process models for large spatial data sets,” *Journal of the Royal Statistical Society: Series B (Statistical Methodology)*, 70, 825–848.

Bhatti, A., Mulla, D., and Frazier, B. (1991), “Estimation of soil properties and wheat yields on complex eroded hills using geostatistics and Thematic Mapper images,” *Remote Sensing of Environment*, 37, 181–191.

Cao, C., Weinreb, M., and Xu, H. (2004), “Predicting simultaneous nadir overpasses among polar-orbiting meteorological satellites for the intersatellite calibration of radiometers,” *Journal of Atmospheric and Oceanic Technology*, 21, 537–542.

Cao, C., Xu, H., Sullivan, J., McMillin, L., Ciren, P., and Hou, Y.-T. (2005), “Intersatellite radiance biases for the High-Resolution Infrared Radiation Sounders (HIRS) on board NOAA-15, -16, and -17 from simultaneous nadir observations,” *Journal of Atmospheric and Oceanic Technology*, 22, 381–395.

Cressie, N. (1993), *Statistics for Spatial Data*, New York: John Wiley & Sons, revised edition.

Cressie, N. and Johannesson, G. (2008), “Fixed rank kriging for very large spatial data sets,” *Journal of the Royal Statistical Society: Series B (Statistical Methodology)*, 70, 209–226.

Datta, A., Banerjee, S., Finley, A. O., and Gelfand, A. E. (2016a), “Hierarchical nearest-neighbor Gaussian process models for large geostatistical datasets,” *Journal of the American Statistical Association*, 111, 800–812.

Datta, A., Banerjee, S., Finley, A. O., Hamm, N. A. S., and Schaap, M. (2016b), “Nonseparable dynamic nearest neighbor Gaussian process models for large spatio-temporal data with an application to particulate matter analysis,” *Ann. Appl. Stat.*, 10, 1286–1316, URL <https://doi.org/10.1214/16-AOAS931>.

Davis, B. M. and Greenes, K. A. (1983), “Estimation using spatially distributed multivariate data: an example with coal quality,” *Journal of the International Association for Mathematical Geology*, 15, 287–300.

Du, J., Zhang, H., Mandrekar, V., et al. (2009), “Fixed-domain asymptotic properties of tapered maximum likelihood estimators,” *the Annals of Statistics*, 37, 3330–3361.

Finley, A. O., Datta, A., Cook, B. D., Morton, D. C., Andersen, H. E., and Banerjee, S. (2019), “Efficient algorithms for Bayesian nearest neighbor Gaussian processes,” *Journal of Computational and Graphical Statistics*, 1–14.

Furrer, R. and Genton, M. G. (2011), “Aggregation-cokriging for highly multivariate spatial data,” *Biometrika*, 98, 615–631.

Furrer, R., Genton, M. G., and Nychka, D. (2006), “Covariance tapering for interpolation of large spatial datasets,” *Journal of Computational and Graphical Statistics*, 15, 502–523.

Genton, M. G. and Kleiber, W. (2015), “Cross-covariance functions for multivariate geostatistics,” *Statistical Science*, 147–163.

Goldberg, M., e. a. (2011), “The Global Space-Based Inter-Calibration Systems,” *Bull. Am. Meteorol. Soc.*, 92, 467–475.

Gramacy, R. B. and Apley, D. W. (2015), “Local Gaussian Process Approximation for Large Computer Experiments,” *Journal of Computational and Graphical Statistics*, 24, 561–578.

Gramacy, R. B. and Lee, H. K. H. (2012), “Cases for the nugget in modeling computer experiments,” *Statistics and Computing*, 22, 713–722.

Han, Z.-H., Zimmermann, R., and Goretz, S. (2010), “A new cokriging method for variable-fidelity surrogate modeling of aerodynamic data,” in *48th AIAA Aerospace sciences meeting including the new horizons forum and Aerospace exposition*.

Hastings, W. K. (1970), “Monte Carlo sampling methods using Markov chains and their applications,” .

Jackson, D., Wylie, D., and Bates, J. (2003), “The HIRS pathfinder radiance data set (1979–2001),” in *Proc. of the 12th Conference on Satellite Meteorology and Oceanography, Long Beach, CA, USA, 10-13 February 2003*, volume 5805 of *LNCS*, Springer.

Katzfuss, M. (2016), “A multi-resolution approximation for massive spatial datasets,” *Journal of the American Statistical Association*. DOI:10.1080/01621459.2015.1123632.

Katzfuss, M. and Guinness, J. (2017), “A general framework for Vecchia approximations of Gaussian processes,” *arXiv preprint arXiv:1708.06302*.

Kaufman, C. G., Schervish, M. J., and Nychka, D. W. (2008), “Covariance tapering for

likelihood-based estimation in large spatial data sets,” *Journal of the American Statistical Association*, 103, 1545–1555.

Kennedy, M. C. and O’Hagan, A. (2000), “Predicting the output from a complex computer code when fast approximations are available,” *Biometrika*, 87, 1–13.

Konomi, B. A. and Karagiannis, G. (2019), “Bayesian analysis of multifidelity computer models with local features and non-nested experimental designs: Application to the WRF model,” Submitted.

Koziel, S., Bekasiewicz, A., Couckuyt, I., and Dhaene, T. (2014), “Efficient multi-objective simulation-driven antenna design using co-kriging,” *IEEE Transactions on Antennas and Propagation*, 62, 5900–5905.

Le Gratiet, L. (2013), “Bayesian analysis of hierarchical multifidelity codes,” *SIAM/ASA Journal on Uncertainty Quantification*, 1, 244–269.

Lindgren, F., Rue, H., and Lindström, J. (2011), “An explicit link between Gaussian fields and Gaussian Markov random fields: the stochastic partial differential equation approach,” *Journal of the Royal Statistical Society: Series B (Statistical Methodology)*, 73, 423–498.

Ma, P., Karagiannis, G., Konomi, B. A., Asher, T. G., Toro, G. R., and Cox, A. T. (2019), “Multifidelity Computer Model Emulation with High-Dimensional Output: An Application to Storm Surge,” .

Matthews, J. L. and Shi, L. (2019), “Intercomparisons of Long-Term Atmospheric Temperature and Humidity Profile Retrievals,” *Remote Sensing*, 11, 853.

National Research Council (2004), *Climate Data Records from Environmental Satellites: Interim Report*, Washington, DC: The National Academies Press, URL <https://www.nap.edu/catalog/10944/climate-data-records-from-environmental-satellites-interim-report>.

Nguyen, H., Cressie, N., and Braverman, A. (2012), “Spatial statistical data fusion for remote sensing applications,” *Journal of the American Statistical Association*, 107, 1004–1018.

— (2017), “Multivariate spatial data fusion for very large remote sensing datasets,” *Remote Sensing*, 9, 142.

Nychka, D., Bandyopadhyay, S., Hammerling, D., Lindgren, F., and Sain, S. (2015), “A multiresolution Gaussian process model for the analysis of large spatial datasets,” *Journal of Computational and Graphical Statistics*, 24, 579–599.

Qian, P. Z. and Wu, C. J. (2008), “Bayesian hierarchical modeling for integrating low-accuracy and high-accuracy experiments,” *Technometrics*, 50, 192–204.

Sang, H. and Huang, J. Z. (2012), “A full scale approximation of covariance functions for large spatial data sets,” *Journal of the Royal Statistical Society: Series B (Statistical Methodology)*, 74, 111–132.

Shi, L., Matthews, J., Ho, S.-p., Yang, Q., and Bates, J. (2016), “Algorithm development

of temperature and humidity profile retrievals for long-term HIRS observations," *Remote Sensing*, 8, 280.

Stein, M. L. (1999), *Interpolation of Spatial Data: Some Theory for Kriging. 2nd edition*, New York: Springer.

— (2014), "Limitations on low rank approximations for covariance matrices of spatial data," *Spatial Statistics*, 8, 1–19.

Stein, M. L., Chi, Z., and Welty, L. J. (2004), "Approximating likelihoods for large spatial data sets," *Journal of the Royal Statistical Society: Series B (Statistical Methodology)*, 66, 275–296.

Taylor-Rodriguez, D., Finley, A. O., Datta, A., Babcock, C., Andersen, H.-E., Cook, B. D., Morton, D. C., and Banerjee, S. (2018), "Spatial Factor Models for High-Dimensional and Large Spatial Data: An Application in Forest Variable Mapping," *arXiv preprint arXiv:1801.02078*.

Vecchia, A. V. (1988), "Estimation and model identification for continuous spatial processes," *Journal of the Royal Statistical Society: Series B (Methodological)*, 50, 297–312.

Ver Hoef, J. M. and Cressie, N. (1993), "Multivariable spatial prediction," *Mathematical Geology*, 25, 219–240.

Williams, C. K. and Rasmussen, C. E. (2006), *Gaussian processes for machine learning*, volume 2, MIT press Cambridge, MA.

## Appendix

### A NNGP specifications

The posterior distribution of

$$\begin{aligned} \tilde{p}(\mathbf{w}_t | \cdot) &\propto \exp \left[ -\frac{1}{2} \sum_{i=1}^{n_t} \left\{ w_t(s_{t,i}) - \mathbf{B}_{t,s_{t,i}} \mathbf{w}_{t,N_t(s_{t,i})} \right\}^T F_{t,s_{t,i}}^{-1} \left\{ w_t(s_{t,i}) - \mathbf{B}_{t,s_{t,i}} \mathbf{w}_{t,N_t(s_{t,i})} \right\} \right] \\ &= \exp \left( -\frac{1}{2} \mathbf{w}_t^T \mathbf{B}_t^T \mathbf{F}_t^{-1} \mathbf{B}_t \mathbf{w}_t \right), \end{aligned} \quad (\text{A.1})$$

where  $\mathbf{F}_t = \text{diag}(F_{t,s_{t,1}}, F_{t,s_{t,2}}, \dots, F_{t,s_{t,n_t}})$ ,  $\mathbf{B}_t = (\mathbf{B}_{t,1}^T, \mathbf{B}_{t,2}^T, \dots, \mathbf{B}_{t,n_t}^T)^T$ , and for each element in  $\mathbf{B}_t$ , we have  $\mathbf{B}_{t,i} = (\mathbf{B}_{t,s_{t,i},1}^T, \mathbf{B}_{t,s_{t,i},2}^T, \dots, \mathbf{B}_{t,s_{t,i},n_t}^T)^T$  and

$$\mathbf{B}_{t,s_{t,i},j} = \begin{cases} 1, & \text{if } i = j, \\ -\mathbf{B}_{t,s_{t,i}}[k], & \text{if } s_{t,j} \text{ is the } k^{\text{th}} \text{ element in } N_t(s_{t,i}), \\ 0, & \text{Others.} \end{cases} \quad (\text{A.2})$$

## B Mean and Variance Specifications

The mean vector  $\boldsymbol{\mu} = (\mu_1(s_{1,1}), \dots, \mu_1(s_{1,n_1}), \dots, \mu_T(s_{T,n_T}))$  is

$$\begin{aligned}\mu_t(s_{t,k}) = & \mathbf{1}_{\{t>1\}}(t) \sum_{i=1}^{t-1} \left\{ \prod_{j=i}^{t-1} \zeta_j(s_{t,k}) \right\} \left\{ \mathbf{h}_i^T(s_{t,k}) \boldsymbol{\beta}_i + \mathbf{1}_{\{s_{t,k} \in \mathbf{S}_i\}}(s_{t,k}) w_i(s_{t,k}) \right\} \\ & + \mathbf{h}_t^T(s_{t,k}) \boldsymbol{\beta}_t + w_t(s_{t,k}),\end{aligned}\quad (\text{B.1})$$

for  $t = 1, \dots, T$ ,  $i = 1, \dots, n_t$ .  $\mathbf{1}_{\{\cdot\}}(\cdot)$  is the indicator function, and covariance matrix  $\boldsymbol{\Lambda}$  is a block matrix with blocks  $\Lambda^{(1,1)}, \dots, \Lambda^{(1,T)}, \dots, \Lambda^{(T,T)}$ , and the size of  $\boldsymbol{\Lambda}$  is  $\sum_{t=1}^T n_t \times \sum_{t=1}^T n_t$ . The  $\Lambda^{(t,t)}$  components are calculated as:

$$\begin{aligned}\Lambda_{k,l}^{(t,t)} = \text{cov}(z_t(s_{t,k}), z_t(s_{t,l}) | \cdot) = & \sum_{i=1}^{t-1} \mathbf{1}_{\{s_{t,k}, s_{t,l} \notin \mathbf{S}_i\}}(s_{t,k}, s_{t,l}) \left\{ \prod_{j=i}^{t-1} \zeta_j(s_{t,k})^T \zeta_j(s_{t,l}) \right\} C_i(s_{t,k}, s_{t,l} | \boldsymbol{\theta}_i) \\ & + \mathbf{1}_{s_{t,k}=s_{t,l}}(s_{t,k}, s_{t,l}) \tau_t^2,\end{aligned}$$

for  $t$  and  $t' = 1, \dots, T$ ;  $k = 1, \dots, n_t$ ;  $l = 1, \dots, n_{t'}$ , and

$$\begin{aligned}\Lambda_{k,l}^{(t,t')} = \text{cov}(z_t(s_{t,k}), z_{t'}(s_{t',l}) | \cdot) = & \sum_{i=1}^{\min(t,t')-1} \mathbf{1}_{\{s_{t,k}, s_{t',l} \notin \mathbf{S}_i\}}(s_{t,k}, s_{t',l}) \left\{ \prod_{j=i}^{\min(t,t')-1} \zeta_j(s_{t,k})^T \zeta_j(s_{t',l}) \right\} \\ & \times C_i(s_{t,k}, s_{t',l} | \boldsymbol{\theta}_i) + \mathbf{1}_{\{s_{t,k}, s_{t',l} \notin \mathbf{S}_{\min(t,t')}\}}(s_{t,k}, s_{t',l}) C_{\min(t,t')}(s_{t,k}, s_{t',l} | \boldsymbol{\theta}_{\min(t,t')}),\end{aligned}\quad (\text{B.2})$$

for  $t \neq t'$ ,  $\Lambda^{(t,t')}$ .

## C Gibbs Sampler

The full conditional distribution of  $\mathbf{w}_1$  is

$$\begin{aligned}w_1(s_u) | \boldsymbol{\Theta}_1, \mathbf{Z}_1 & \sim N(V_{\mathbf{w}_1}(s_u) \mu_{\mathbf{w}_1}(s_u), V_{\mathbf{w}_1}(s_u)), \\ V_{\mathbf{w}_1}(s_u) & = (F_{1,s_u}^{-1} + \tau_1^{-2})^{-1}, \\ \mu_{\mathbf{w}_1}(s_u) & = \tau_1^{-2} [z_1(s_u) - \mathbf{h}_1^T(s_u) \boldsymbol{\beta}_1] + F_{1,s_u}^{-1} \mathbf{B}_{1,s_u} \mathbf{w}_{1,N_1(s_u)},\end{aligned}\quad (\text{C.1})$$

for  $s_u \in \mathbf{S}_1$ .

With the specification of priors, the posterior distributions of the parameters are:

$$\begin{aligned}\boldsymbol{\beta}_t | \mathbf{w}_t, \tilde{\mathbf{y}}_{t-1}, \boldsymbol{\gamma}_{t-1}, \tau_t, \mathbf{Z}_t & \sim N(\mathbf{V}_{\boldsymbol{\beta}_t}^* \boldsymbol{\mu}_{\boldsymbol{\beta}_t}^*, \mathbf{V}_{\boldsymbol{\beta}_t}^*), \\ \boldsymbol{\gamma}_t | \tilde{\mathbf{y}}_t, \boldsymbol{\beta}_{t+1}, \tau_{t+1}, \mathbf{Z}_{t+1} & \sim N(\mathbf{V}_{\boldsymbol{\gamma}_t}^* \boldsymbol{\mu}_{\boldsymbol{\gamma}_t}^*, \mathbf{V}_{\boldsymbol{\gamma}_t}^*),\end{aligned}$$

$$\begin{aligned} \sigma_t^2 | \tilde{\mathbf{w}}_t, \phi_t &\sim IG(a_{\sigma_t}^*, b_{\sigma_t}^*), \\ \tau_t | \beta_t, \mathbf{w}_t, \tilde{\mathbf{y}}_{t-1}, \mathbf{Z}_t, \gamma_{t-1} &\sim IG(a_{\tau_t}, b_{\tau_t}), \end{aligned} \quad (C.2)$$

For  $\beta_t$ , we have:

$$\begin{aligned} p(\beta_t | \cdot) &\propto N(\beta_t | \mu_{\beta_t}, \mathbf{V}_{\beta_t}) \times N(\mathbf{Z}_t | \mathbf{1}_{t>1}(t) \zeta_{t-1} \circ y_{t-1}(\mathbf{S}_t) + \delta_t, \tau_t \mathbf{I}) \\ &\propto \exp \left\{ -\frac{1}{2} (\beta_t - \mu_{\beta_t})^T \mathbf{V}_{\beta_t}^{-1} (\beta_t - \mu_{\beta_t}) \right\} \times \\ &\quad \exp \left[ -\frac{1}{2\tau_t^2} \left\{ \mathbf{Z}_t - \mathbf{1}_{t>1}(t) \zeta_{t-1} \circ y_{t-1}(\mathbf{S}_t) - \delta_t \right\}^T \left\{ \mathbf{Z}_t - \mathbf{1}_{t>1}(t) \zeta_{t-1} \circ y_{t-1}(\mathbf{S}_t) - \delta_t \right\} \right] \\ &\propto \exp \left\{ -\frac{1}{2} \left\{ \mathbf{V}_{\beta_t}^{-1} + \frac{1}{\tau_t^2} \mathbf{h}_t \mathbf{h}_t^T \right\} \beta_t^T \beta_t + \right. \\ &\quad \left. \left[ \mu_{\beta_t}^T \mathbf{V}_{\beta_t}^{-1} + \frac{1}{\tau_t^2} (\mathbf{Z}_t - \mathbf{1}_{t>1}(t) \zeta_{t-1} \circ y_{t-1}(\mathbf{S}_t) - \mathbf{w}_t)^T \mathbf{h}_t^T \right] \beta_t \right\}, \end{aligned}$$

and we have:

$$\begin{aligned} \beta_t | \mathbf{w}_t, \tilde{\mathbf{y}}_{t-1}, \gamma_{t-1}, \tau_t, \mathbf{Z}_t &\sim N(\mathbf{V}_{\beta_t}^* \mu_{\beta_t}^*, \mathbf{V}_{\beta_t}^*), \\ \mu_{\beta_t}^* &= \mu_{\beta_t}^T \mathbf{V}_{\beta_t}^{-1} + \frac{1}{\tau_t^2} (\mathbf{Z}_t - \mathbf{1}_{t>1}(t) \zeta_{t-1} \circ y_{t-1}(\mathbf{S}_t) - \mathbf{w}_t)^T \mathbf{h}_t^T, \\ \mathbf{V}_{\beta_t}^* &= \left( \mathbf{V}_{\beta_t}^{-1} + \frac{1}{\tau_t^2} \mathbf{h}_t \mathbf{h}_t^T \right)^{-1}, \end{aligned} \quad (C.3)$$

where  $\mathbf{1}_{t>1}(t)$  is an indicator function equals 1 for  $t > 1$ , otherwise 0. The full conditional distribution for parameter  $\sigma_t^2$  is:

$$p(\sigma_t^2 | a_t, b_t, w_t(\tilde{\mathbf{S}}_t), \phi_t) \propto IG(a_t, b_t) \times \tilde{p}(\mathbf{w}_t) \times \tilde{p}(w_t(\mathbf{S}_t^*) | \mathbf{w}_t).$$

From nearest neighbor Gaussian process approach, we have

$$\begin{aligned} \tilde{p}(\mathbf{w}_t) &= \prod_{i=1}^{n_t} p(w_t(s_{t,i}) | \mathbf{w}_{t,N_t(s_{t,i})}), \\ w_t(s_{t,i}) | \mathbf{w}_{t,N_t(s_{t,i})} &\sim N(\mathbf{B}_{s_{t,i}} \mathbf{w}_{t,N_t(s_{t,i})}, F_{s_{t,i}}), \end{aligned}$$

where  $\mathbf{B}_{s_{t,i}} = \mathbf{C}_{s_{t,i}, N(s_{t,i})}^T \mathbf{C}_{N(s_{t,i})}^{-1}$ ,  $F_{s_{t,i}} = \mathbf{C}_{s_{t,i}, s_{t,i}} - \mathbf{C}_{s_{t,i}, N(s_{t,i})}^T \mathbf{C}_{N(s_{t,i})}^{-1} \mathbf{C}_{s_{t,i}, N(s_{t,i})}$ , here  $\mathbf{C}$  is the covariance matrix. Denote  $\mathbf{C}_t(\cdot, \cdot | \sigma_t^2, \phi_t) = \sigma_t^2 \boldsymbol{\rho}_t(\cdot, \cdot | \phi_t)$ , we have:

$$\mathbf{F}_{s_{t,i}} = \sigma_t^2 (\boldsymbol{\rho}(s_{t,i}, s_{t,i}) - \boldsymbol{\rho}_{s_{t,i}, N(s_{t,i})} \boldsymbol{\rho}_{N(s_{t,i})}^{-1} \boldsymbol{\rho}_{s_{t,i}, N(s_{t,i})}) = \sigma_t^2 \tilde{\mathbf{F}}_{s_{t,i}},$$

and the following full conditional distribution for  $\sigma_t^2$  is:

$$\begin{aligned}
p(\sigma_t^2 | a_t, b_t, \tilde{\mathbf{w}}_t, \boldsymbol{\phi}_t) &\propto (\sigma_t^2)^{-a_t-1} \exp\left(-\frac{b_t}{\sigma_t^2}\right) \times \tilde{p}(\mathbf{w}_t) \times \tilde{p}(w_t(\mathbf{S}_t^*) | \mathbf{w}_t) \\
&\propto (\sigma_t^2)^{-a_t-1-\frac{1}{2}(n_t+n_t^*)} \exp\left[-\frac{1}{2\sigma_t^2} \sum_{i=1}^{n_t} \left\{w_t(s_{t,i}) - \mathbf{B}_{s_{t,i}} \mathbf{w}_{t,N_t(s_{t,i})}\right\}^T (\tilde{F}_{s_{t,i}})^{-1} \left\{w_t(s_{t,i}) - \mathbf{B}_{s_{t,i}} \mathbf{w}_{t,N_t(s_{t,i})}\right\}\right. \\
&\quad \left.- \frac{1}{2\sigma_t^2} \sum_{i=1}^{n_t^*} \left\{w_t(s_{t,i}^*) - \mathbf{B}_{s_{t,i}^*} \mathbf{w}_{t,N_t(s_{t,i}^*)}\right\}^T (\tilde{F}_{s_{t,i}^*})^{-1} \left\{w_t(s_{t,i}^*) - \mathbf{B}_{s_{t,i}^*} \mathbf{w}_{t,N_t(s_{t,i}^*)}\right\} - \frac{b_t}{\sigma_t^2}\right],
\end{aligned}$$

which is a  $IG(a_t^*, b_t^*)$  distribution and

$$\begin{aligned}
a_{\sigma_t}^* &= a_t + \frac{1}{2}(n_t + n_t^*), \\
b_{\sigma_t}^* &= b_t + \frac{1}{2} \sum_{i=1}^{n_t} \left\{w_t(s_{t,i}) - \mathbf{B}_{s_{t,i}} \mathbf{w}_{t,N_t(s_{t,i})}\right\}^T (\tilde{F}_{s_{t,i}})^{-1} \left\{w_t(s_{t,i}) - \mathbf{B}_{s_{t,i}} \mathbf{w}_{t,N_t(s_{t,i})}\right\} \\
&\quad + \frac{1}{2} \sum_{i=1}^{n_t^*} \left\{w_t(s_{t,i}^*) - \mathbf{B}_{s_{t,i}^*} \mathbf{w}_{t,N_t(s_{t,i}^*)}\right\}^T (\tilde{F}_{s_{t,i}^*})^{-1} \left\{w_t(s_{t,i}^*) - \mathbf{B}_{s_{t,i}^*} \mathbf{w}_{t,N_t(s_{t,i}^*)}\right\}. \tag{C.4}
\end{aligned}$$

For  $\tau_t$ , we have the full conditional distribution for each level:

$$p(\tau_t | \cdot) = IG(\tau_t | c_t, d_t) \times \prod_{i=1}^{n_t} N(\mathbf{Z}_t | \cdot).$$

This structure gives us the inverse gamma distribution with:

$$\begin{aligned}
p(\tau_t | \cdot) &\sim IG(a_{\tau_t}^*, b_{\tau_t}^*) \\
a_{\tau_t}^* &= c_t + \frac{1}{2}n_t, \\
b_{\tau_t}^* &= d_t + \frac{1}{2} \sum_{u \in \mathbf{S}_t} (z_t(s_u) - \zeta_{t-1}(s_u)y_{t-1}(s_u) - \delta_t(s_u))^2. \tag{C.5}
\end{aligned}$$

For  $\boldsymbol{\gamma}_t$ , we have:

$$\begin{aligned}
p(\boldsymbol{\gamma}_t | \cdot) &\propto N(\boldsymbol{\gamma}_t | \boldsymbol{\mu}_{\boldsymbol{\gamma}_t}, \mathbf{V}_{\boldsymbol{\gamma}_t}) \times N(\mathbf{Z}_{t+1} | \mathbf{g}_t^T \boldsymbol{\gamma}_t y_t(\mathbf{S}_{t+1}) + \mathbf{h}_{t+1} \boldsymbol{\beta}_{t+1} + \mathbf{w}_{t+1}, \tau_{t+1} \mathbf{I}) \\
&\propto \exp\left\{-\frac{1}{2}(\boldsymbol{\gamma}_t - \boldsymbol{\mu}_{\boldsymbol{\gamma}_t})^T \mathbf{V}_{\boldsymbol{\gamma}_t}^{-1} (\boldsymbol{\gamma}_t - \boldsymbol{\mu}_{\boldsymbol{\gamma}_t})\right\} \times \\
&\quad \exp\left[-\frac{1}{2\tau_{t+1}^2} \left\{\mathbf{Z}_{t+1} - \mathbf{g}_t^T \boldsymbol{\gamma}_t y_t(\mathbf{S}_{t+1}) - \boldsymbol{\delta}_{t+1}\right\}^T \left\{\mathbf{Z}_{t+1} - \mathbf{g}_t^T \boldsymbol{\gamma}_t y_t(\mathbf{S}_{t+1}) - \boldsymbol{\delta}_{t+1}\right\}\right] \\
&\propto \exp\left[-\frac{1}{2} \boldsymbol{\gamma}_t^T \mathbf{V}_{\boldsymbol{\gamma}_t}^{-1} \boldsymbol{\gamma}_t - \frac{1}{2\tau_{t+1}^2} y_t(\mathbf{S}_{t+1})^T y_t(\mathbf{S}_{t+1}) (\mathbf{g}_t^T \boldsymbol{\gamma}_t)^T (\mathbf{g}_t^T \boldsymbol{\gamma}_t) + \right]
\end{aligned}$$

$$\left\{ \boldsymbol{\mu}_{\gamma_t}^T \mathbf{V}_{\gamma_t}^{-1} + \frac{1}{\tau_{t+1}^2} \left[ (\mathbf{Z}_{t+1} - \boldsymbol{\delta}_{t+1})^T y_t(\mathbf{S}_{t+1}) \right] \mathbf{g}_t^T \right\} \gamma_t \Big]$$

so that:

$$\begin{aligned} \boldsymbol{\gamma}_t | \tilde{\mathbf{y}}_t, \boldsymbol{\beta}_{t+1}, \tau_{t+1}, \mathbf{Z}_{t+1} &\sim N(\mathbf{V}_{\gamma_t}^* \boldsymbol{\mu}_{\gamma_t}^*, \mathbf{V}_{\gamma_t}^*), \\ \boldsymbol{\mu}_{\gamma_t}^* &= \boldsymbol{\mu}_{\gamma_t}^T \mathbf{V}_{\gamma_t}^{-1} + \frac{1}{\tau_{t+1}^2} \left[ (\mathbf{Z}_{t+1} - \boldsymbol{\delta}_{t+1})^T y_t(\mathbf{S}_{t+1}) \right] \mathbf{g}_t^T, \\ \mathbf{V}_{\gamma_t}^* &= \left( \mathbf{V}_{\gamma_t}^{-1} + \frac{1}{\tau_{t+1}^2} y_t(\mathbf{S}_{t+1})^T y_t(\mathbf{S}_{t+1}) \mathbf{g}_t \mathbf{g}_t^T \right)^{-1}. \end{aligned} \quad (\text{C.6})$$

For a new input location  $s_p \notin \tilde{\mathbf{S}}_t$ , we have the predictive distribution of  $w_t(s_p)$ :

$$\begin{aligned} w_t(s_p) &\sim N(V_{t,s_p} \mu_{t,s_p}, V_{t,s_p}), \\ V_{t,s_p} &= (\tau_t^{-2} + \tilde{F}_{t,s_p}^{-1})^{-1}, \\ \mu_{t,s_p} &= \tau_t^{-2} [z_t(s_p) - \mathbf{h}_t^T(s_p) \boldsymbol{\beta}_t - \zeta_{t-1}(s_p) y_{t-1}(s_p)] + \tilde{F}_{t,s_p}^{-1} \tilde{\mathbf{B}}_{t,s_p} \tilde{\mathbf{w}}_{t,\tilde{N}_t(s_p)}, \quad t = 1, 2, \dots, T-1, \end{aligned} \quad (\text{C.7})$$

with  $\tilde{\mathbf{B}}_{t,s_p} = \mathbf{C}_{s_p, \tilde{N}_t(s_p)}^T \mathbf{C}_{\tilde{N}_t(s_p)}^{-1}$ ,  $\tilde{F}_{t,s_p} = \mathbf{C}(s_p, s_p) - \mathbf{C}_{s_p, \tilde{N}_t(s_p)}^T \mathbf{C}_{\tilde{N}_t(s_p)}^{-1} \mathbf{C}_{s_p, \tilde{N}_t(s_p)}$ ,  $\tilde{N}_t(s_p)$  is the m nearest neighbors in  $\tilde{\mathbf{S}}_{t,< p}$ , and  $\tilde{\mathbf{w}}_{t,\tilde{N}_t(s_p)}$  is the corresponding nearest neighbor subset of  $\tilde{\mathbf{w}}_t$ .

## D Performance Metrics

In the empirical comparisons, we used the following performance metrics:

1. Root mean square prediction error (RMSPE) is defined as

$$\text{RMSPE} = \sqrt{\frac{1}{n} \sum_{i=1}^n (y_i^{\text{pred}} - y_i^{\text{obs}})^2}$$

where  $y^{\text{obs}}$  is the observed value in test data-set and  $y_i^{\text{pred}}$  is the predicted value from the model. It measures the accuracy of the prediction from model. Smaller values of RMSPE indicate more accurate model.

2. Nash-Sutcliffe model efficiency coefficient (NSME) is defined as:

$$\text{NSME} = 1 - \frac{\sum_{i=1}^n (y_i^{\text{pred}} - y_i^{\text{obs}})^2}{\sum_{i=1}^n (y_i^{\text{obs}} - \bar{y}^{\text{obs}})^2}$$

where  $y^{\text{obs}}$  is the observed value in test data-set and  $y_i^{\text{pred}}$  is the predicted value from the model. NSME gives the relative magnitude of the residual variance from data and

the model variance. NSME values closer to 1 indicate that the model has a better predictive performance.

3. 95% CVG is the coverage probability of 95% equal tail prediction interval. 95% CVG values closer to 0.95 indicate better prediction performance for the model.
4. 95% ALCI is average length of 95% equal tail prediction interval. Smaller 95% ALCI values indicate better prediction performance for the model.
5. Deviance information criterion (DIC) and the effective number of parameters of the model( $p_D$ ) are defined as:

$$\begin{aligned} D(\theta) &= -2\log(p(y|\theta)) + C, \\ p_D &= \overline{D(\theta)} - D(\bar{\theta}), \\ \text{DIC} &= p_D + \overline{D(\theta)} \end{aligned}$$

It is used in Bayesian model selection. Models with smaller DIC and  $p_D$  are preferable.